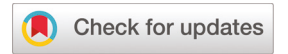
Analyst



PAPER View Article Online View Journal



Cite this: DOI: 10.1039/d2an00724j

Impact of physical and chemical parameters on square wave anodic stripping voltammetry for trace Pb²⁺ detection in water†

Connor E Rahm, Pankaj Gupta, Vandna K. Gupta, D Artur Huseinov, Ben Griesmer and Noe T. Alvarez*

Exposure to lead, a toxic heavy metal, in drinking water is a worldwide problem. Lead leaching from lead service lines, the main contamination source, and other plumbing materials is controlled by the plumbosolvency of water. Square wave anodic stripping voltammetry (SWASV) has been greatly explored as a rapid and portable technique for the detection of trace Pb2+ ions in drinking water. However, the impact of water quality parameters (WQP) on the SWASV technique is not well understood. Herein, SWASV was employed to detect 10 μ g L⁻¹ Pb²⁺ and determine trends in the stripping peak changes in simulated water samples while individually varying the pH, conductivity, alkalinity, free chlorine, temperature, and copper levels. The pH and conductivity were controlled using the buffer 3-(N-morpholino)propanesulfonic acid (MOPS), and NaNO₃, respectively and kept at pH = 7.0 and conductivity = $500 \mu S cm^{-1}$ when exploring other WQPs. The working electrode, a gold-nanoparticle-modified carbon nanotube fiber cross-section (AuNP-CNTf-CS) electrode provided sufficiently sharp and prominent peaks for 10 μ g L⁻¹ Pb²⁺ detection as well as good reproducibility, with a relative error of 5.9% in simulated water. We found that conductivity, and temperature had a proportional relationship to the peak height, and pH, alkalinity, free chlorine, and copper had an inverse relationship. In addition, increasing the copper concentration caused broadening and shifting of the Pb²⁺ stripping peak. At extremely low conductivities (<100 µS cm⁻¹), the voltammograms became difficult to interpret owing to the formation of inverted and distorted peaks. These trends were then also observed within a local drinking water sample in order to validate the results.

Received 27th April 2022, Accepted 21st June 2022 DOI: 10.1039/d2an00724j

rsc.li/analyst

1. Introduction

Lead in drinking water is a current global issue because of its toxicity to humans. Lead is rarely present in natural water sources, instead originating from lead pipes and materials used in century-old plumbing and water distribution systems. The primary source of Pb²⁺ leaching into drinking water is premise plumbing material that contains lead in the pipes, joints, solder, brass couplings, and faucets. To Some plumbing materials containing polyvinyl chloride (PVC) and polypropylene have also been found to release lead at levels up to 113 and 40 $\mu g \; L^{-1} \; Pb^{2+}$, respectively. Continuous exposure to trace amounts of lead can cause adverse health effects in multiple organs and systems such as the liver, kidney, repro-

from the ability of Pb2+ ions to disrupt normal biological functions by binding to various protein sites and ligands containing oxygen, nitrogen, and sulfur. 13,14 In children lead consumption at trace concentrations over time can have detrimental long-term effects on the developing central nervous system, resulting in irreversibly diminished IQ levels.¹⁵ The World Health Organization (WHO) and the United States Environmental Protection Agency (US EPA) have set maximum contaminant levels (MCL) and action levels of 10 and 15 µg L⁻¹ Pb²⁺, respectively.^{2,16,17} Lead levels in municipal waters are monitored by local water supply systems (WSSs) and regulated by government agencies worldwide to protect civilians from exposure through drinking water. However, owing to lead leaching from premise plumbing materials, the lead levels in drinking water in homes, schools, and office buildings may be higher than those monitored by WSSs.5 In the United States, the Lead and Copper Rule (LCR) requires WSSs to adjust the physical and chemical properties of distributed water to decrease the plumbosolvency,18 which is the ability of water to

leach Pb²⁺ from plumbing materials.

ductive system, and nervous system. 9-12 This toxicity originates

Department of Chemistry, University of Cincinnati, Cincinnati, OH 45221, USA. E-mail: alvarene@ucmail.uc.edu; Tel: +1 513-556-9370

[†] Electronic supplementary information (ESI) available: Electrode materials characterization; impedance, Raman spectra, electrochemical characterization and optimization of microelectrodes. See DOI: https://doi.org/10.1039/d2an00724j

Conventionally, lead and other heavy metal ions (HMIs) have been detected using inductively coupled plasma massspectrometry (ICP-MS) and atomic absorption spectroscopy (AAS). Although highly sensitive, these techniques are labor intense, expensive, and reliant on non-portable instrumentation that requires frequent maintenance and trained lab personnel. 19,20 The issue of lead leaching from premise plumbing demands a sensitive detection technique that is simple, rapid, and capable of repeated analyses by consumers. 21 Square wave anodic stripping voltammetry (SWASV) is a powerful electroanalytical technique commonly used to detect HMIs, 22,23 and is affordable, portable, user-friendly, and capable of directly and rapidly determining Pb2+ in potable water. 24,25 SWASV is a multi-step technique consisting of a reductive preconcentration step, an oxidative stripping step, and sometimes a cleaning step. HMIs of interest are electrochemically reduced at the working electrode surface, and then an oxidative potential scanning step is performed. The resulting current responses can be attributed to specific metals based on their redox potentials and the Nernst equation.²⁶ The major drawback of the SWASV technique is that lead needs to be in an electrochemically reducible state in solution.²⁷ Water quality parameters (WOPs) such as pH, conductivity, alkalinity, temperature and free chlorine can influence the oxidation state and solubility of lead in drinking water, 28-30 thus affecting the preconcentration step of SWASV as well as its sensitivity, which is in part due to the accumulation of the analyte on the electrode surface. Therefore, it is common practice to adjust the pH and conductivity of a water sample before analysis. Although the optimal buffer, molarity, and pH have been investigated for a multitude of electrodes, 23 the effects of various WOPs on the SWASV technique for Pb²⁺ detection in unaltered drinking water are not well understood.³¹ There is a need to understand the impact of these WOPs on the SWASV technique for detecting Pb2+ without the addition or dilution with supporting electrolyte, representing each WQP from expected concentration ranges reported for real water samples.

The physical and chemical WQPs regularly monitored by WSSs include pH, conductivity, alkalinity, hardness, dissolved inorganic carbon, total organic carbon, temperature, chlorine, color, turbidity, bromate boron, total dissolved solids, heavy metals, anion and cation concentrations.³² The WQPs of tap water vary with location, season, anthropogenic activity, and source (ground or surface water),³² affecting the applicability of the SWASV technique for HMI detection.³¹ The solubility of Pb²⁺ ions increases at lower pH values, as revealed by equilibrium models such as the Pourbaix diagrams of lead with various compounds as well as lead pipe scale and coupon studies. 28,33 As crucial WQPs, water hardness and alkalinity are expressed as mg L-1 CaCO3, but they represent various chemical species in water.34 Water hardness is a measure of the concentration of divalent cations, mainly of calcium and magnesium ions, and indicates the tendency to form soap scum and scale, which precipitates when water is boiled.³⁴ Alkalinity is the acid neutralizing capacity of water, which is mainly attributed to hydrocarbonate (HCO₃⁻), carbonate

(CO₃²⁻), hydroxide (OH⁻), ammonia (NH₄⁺), and phosphate (PO₄³⁻) ions.^{34,35} The alkalinity of water decreases plumbosolvency and Pb2+ ion solubility by stabilizing scale precipitation, preventing lead leaching, and increasing buffer capacity. 30,36 Water conductivity represents the total ion concentration, including Ca2+, Mg2+, Na+, and K+ as significant cations and HCO₃⁻, SO₄²⁻, and Cl⁻ as significant anions.³⁷ The conductivities of water sources vary naturally depending on environment and season due to three main processes: evaporation/ precipitation, rock and mineral erosion, and atmospheric precipitation and degassing of ions. 37,38 These variations can become an issue when using electrochemical analysis techniques because ohmic drop occurs at lower solution conductivities.39

To control biological activity, the US EPA requires the addition of disinfectants to drinking water. 16 As the most common disinfectant, chlorine is used as a biocide to control microbes in drinking water,29 and the US EPA has set the maximum allowable free chlorine level in drinking water at 4.0 mg L⁻¹ (as Cl₂).⁴⁰ Free chlorine is the amount of active chlorine present in water that can oxidize potential biological contaminants or react with organic pollutants and metal plumbing.41 Various compounds can form free chlorine, including chlorine gas, sodium hypochlorite, and chloramines,35 and the concentration of free chlorine decreases as water moves through the distribution system. Temperature is a critical WQP that influences many of the other WQPs and affects chemical and biological processes. 42 High temperatures have been reported to increase lead leaching, 43 chlorine decay rates, toxic disinfection byproduct levels, and biological activity.42 To control biological activity in drinking water the WHO recommends water temperatures be below 20 °C, while avoiding those in the range of 25-60 °C.44 Copper from the corrosion of copper plumbing materials has been found as a metal contaminant in drinking water at concentrations of 0-3000 μg L⁻¹. The US EPA, which regulates copper under the Safe Drinking Water Act (SDWA), has set an MCL of 1300 $\mu g L^{-1}$ copper. 16 These water parameters were chosen to study the influence on the Pb2+ detection of the SWASV technique because of their potential for influencing the speciation of Pb²⁺. To our knowledge, the effect of these parameters on the SWASV technique for point of care trace Pb2+ detection have not been addressed. The traditional way to analyze water samples for lead is to dilute the drinking water sample in a supporting electrolyte buffer, and the sample complexity is not taken into consideration. Understanding how different WQPs influence the SWASV technique will assist researchers expand the applicability for direct lead detection at drinking water sources.

Carbon nanotubes (CNTs) are an ideal working electrode material for the SWASV technique owing to their electrical conductivity, 45,46 robustness over a wide potential window, 24 fast electron transfer, 45 high mechanical strength, and easily modifiable surface functionalities. 47 CNTs in the form of fibers, 25 nanoelectrode ensembles, 48 cross sections, 49 printed films,²⁴ and thin films⁵⁰ have been used as working electrodes

for electroanalytical sensing applications. Furthermore, increased sensitivity for HMI detection has been achieved by drop-casting dispersed multi-walled carbon nanotubes (MWCNTs) onto glassy carbon and screen-printed carbon electrodes. 47,51 Gold-modified working electrodes have also been well studied using SWASV for the detection of HMIs. 52,53 During the SWASV analysis of HMIs, gold electrodes exhibit underpotential deposition (UPD), 54,55 where the potential at which the target metal ion is reduced on the electrode surface is more positive than the Nernst potential. This phenomenon is due to the interaction energy between the gold electrode and the metal of interest (gold-metal) being greater than that between the deposited metal and the metal ion of interest (bulk metal - metal).⁵⁴ During UPD, a monolayer of the target metal is formed on the gold surface, followed by regular bulk metal deposition, which leads to two or more stripping peaks and thus complicates data interpretation. Nevertheless, UPD-SWASV provides increased sensitivity to trace metals while shortening deposition times and lowering deposition potentials.

In this work, we report the effects of six WQPs (pH, conductivity, chlorine, hardness, temperature, and copper) on the SWASV technique for detecting 10 µg L⁻¹ Pb²⁺ in simulated drinking water samples. To our knowledge it is the first attempt trying to understand how the SWASV technique will perform due to the complexity of drinking water samples. The WQP ranges were selected by considering the values reported in drinking water supplies and the guidelines set by the US EPA. For the working electrode, a bare carbon nanotube fiber cross-section (CNTf-CS) microelectrode reported previously by our group^{45,49} was modified with gold to ensure robustness and longevity. The gold-nanoparticle-modified CNT fiber cross-section (AuNP-CNTf-CS) microelectrode consisted of six individual ~70 µm densified CNT fibers embedded in a polymer capsule and sliced to ~100 μm thick cross sections. The obtained insights into the influence of various WQPs on the performance of the ASV technique will allow the design of better electrochemical detection systems and protocols for the effective evaluation of drinking water systems. The applicability of the results found in the simulated water samples were tested by studying changes of the WQPs in a local drinking water (LDW) sample.

2. Experimental

2.1. Chemicals and reagents

Pb $^{2+}$ and Cu $^{2+}$, and CaCO $_3$ solutions (99.95–100.5%, TraceCERT ICP standard grade), 3-(*N*-morpholino)propanesulfonic acid (MOPS, \geq 99.5%, ACS reagent grade), NaClO $^-$ (4.00–5.99% reagent grade), NaNO $_3$ (\geq 99.0%, ReagentPlus), NaCH $_3$ COOH (\geq 99.0%, BioXtra), NaOH (\geq 99.0%, ACS reagent grade), KCl (\geq 99.0%, BioXtra), KAuCl $_4$ (98%), [Ru(NH $_3$) $_6$]Cl $_3$ (98%), eriochrome black T (ACS reagent grade), and ethylene-diaminetetracetic acid disodium salt dihydrate (99.0–101.0% titration) were all purchased from Sigma Aldrich. Fast-drying

silver paint and clear weld epoxy resin were obtained from Ted-Pella Inc. (Redding, CA) and JB Weld, respectively. Embedded CNTf cross sections were prepared using an EMBed-812 embedding kit (Electron Microscopy Sciences, PA, USA) which consisted of EMBed-812 resin, dodecenyl succinic anhydride, methyl-5-norbornene-2,3-dicarboxylic anhydride, and n-benzyldimethylamine. Chemical vapor deposition was used to synthesize drawable vertically aligned CNT forests as reported previously by our group, 56,57 using ultrapure ethylene (Wright Brothers, USA) as the carbon source and Fe/Co (Goodfellow, USA) as the catalyst. All solutions were prepared in Milli-Q ultra-pure deionized (DI) water (\leq 18.2 M Ω cm).

2.2. Instrumentation and electrochemical cell

A BASi Epsilon Eclipse™ Model EF-1031electrochemical analyzer (Lafayette, IN) was used for voltammetric experiments, including cyclic voltammetry (CV) modifications and analysis, SWASV in simulated WQP samples, and controlled potential electrolysis (CPE) cleaning processes at room temperature, unless otherwise stated. SWASV experiments were performed in a 50 mL Teflon beaker containing 40 mL of a simulated water sample. The three-electrode electrochemical cell was used for voltammetric experiments with a platinum wire auxiliary electrode, a Ag/AgCl (3 M NaCl) (ALS Co., Ltd, Model 012,167 RE-1B) glass capillary reference electrode, and an AuNP-CNTf-CS working electrode, unless otherwise stated. Electrochemical impedance spectroscopy (EIS) was performed using a Gamry Instruments Reference 600 potentiostat/galvanostat/ZRA to characterize the modified AuNP-CNTf-CS and bare CNTf-CS electrodes. Scanning electron microscopy (SEM) and energy-dispersive X-ray analysis (EDAX) were performed using a FEI Apreo 2 C system (Thermo Scientific) to characterize the electrodes and confirm gold modification on the surface of the AuNP-CNTf-CS electrode. Elemental identification was performed and weight percentages were calculated using the TEAMTM eZAF EDS Smart Quant software. Raman spectra were collected using a Renishaw in via Raman microscope system (West Dundee, IL, USA) to characterize the gold particles on the modified AuNP-CNTf-CS electrode.

2.2.1. Simulated water sample WQP preparation. The WQP test solutions were prepared using a standard stock solution of 0.1 M MOPS buffer (pH = 7.0) with a conductivity of \sim 500 μ S cm⁻¹ in DI water, unless otherwise stated. To study the pH effect, simulated water samples were prepared by adjusting pH of the stock solutions to 6.0, 6.5, 7.0, 7.5, and 8.0 using 5.0 M NaOH and 5.0 M HNO3. To study the effect of conductivity, simulated water samples were prepared by adjusting the conductivity of the stock solutions to 100, 300, 500, 700, and 900 μS cm⁻¹ using 5.0 M NaNO₃. The effect of free chlorine was studied by adding a working solution of NaClO to 40 mL of the stock solution to obtain simulated water samples with free chlorine levels of 1.0, 2.0, 3.0, and 4.0 mg L⁻¹ (0.1 M MOPS; pH = 7.0; conductivity = $500 \mu \text{S cm}^{-1}$). The effect of alkalinity was investigated by adding solid CaCO3 into 250 mL stock solutions (0.1 M MOPS; pH = 7.0; conductivity = 500 μS cm⁻¹) to obtain simulated water samples with 0, 50, 100, 150,

200, 250, 300, and 350 mg L^{-1} CaCO₃, CO₂(g) was bubbled into each solution for 30 minutes to ensure the dissolution of calcium carbonate into Ca2+ and HCO3- ions, discussed in more detail in section 3.6. To study the effect of temperature, the stock solution (0.1 M MOPS; pH = 7.0; conductivity = 500 μS cm⁻¹) was heated or cooled to 10, 20, 30, and 40 °C using a 1000 mL jacketed glass beaker containing DI water as a water bath. The bath level was sufficient to control the temperature of the simulated water sample in the Teflon beaker without overflowing into it. The sample in the electrochemical cell was allowed to reach equilibrium at the desired temperature before performing SWASV measurements. The effect of copper was studied by adding Cu2+ into 40 mL volumes of the stock solution (0.1 M MOPS; pH = 7.0; conductivity = 500 µS cm⁻¹) to obtain simulated water solutions with copper levels of 0, 10, 50, 100, 200, 500, and 1000 μg L⁻¹. All WQP testing was performed within one week of preparing working and stock solutions. However, the free chlorine simulated water samples were analyzed immediately after preparation. All WQP testing was performed without their dilution into a supporting electrolyte buffer solution.

2.2.2 Local drinking water sample collection. A local drinking water (LDW) sample was collected from a potable water source into a HDPE bottle without any post treatment. The pH, conductivity, alkalinity, free chlorine, copper, and lead levels were analyzed are reported in ESI Table S1.† The LDW sample was tested without the addition of any supporting electrolyte buffer and then the pH, conductivity, alkalinity, free chlorine, temperature, copper, and lead were adjusted following the same procedure as the one employed in the simulated water sample WQP preparation.

2.3. SWASV procedure

2.3.1. SWASV parameters. Electrochemical analysis of 10 μg L⁻¹ Pb²⁺ in the WQP samples was carried out on the AuNP-CNTf-CS microelectrode by employing SWASV. The stripping potential window was -800 mV to +300 mV with a frequency of 15 Hz, an amplitude of 25 mV, a deposition time of 120 s, a quiet time of 10 s, and a deposition potential of -800 mV, unless otherwise stated.

2.3.2. Simulated water sample WQP analysis. For each WQP, the SWASV measurements were performed using the same procedure, unless otherwise stated. Each of the six WQPs were evaluated using a separate electrode to reduce experimental error due to variations in the electrode surface area, and a single working electrode was employed for the individual WQP being studied. For each AuNP-CNTf-CS electrode, CV (200 to -400 mV at 100 mV s⁻¹) was performed in the standard 0.1 M MOPS to remove any contaminants and precondition the electrode surface before SWASV experiments. Before being used to evaluate the WQP samples, each electrode was tested in the standard solution (0.1 M MOPS, pH = 7.0, conductivity = 500 μ S cm⁻¹) without Pb²⁺ to collect a baseline (n = 3) and with 10 µg L⁻¹ Pb²⁺ to determine the normal response of the electrode to trace Pb²⁺. Between each SWASV measurement, a 60 s CPE process was performed at +500 mV in the test solution with stirring. A fresh 40 mL working solution was prepared for each variable change within a WQP study. These samples were tested without the addition of concentrated supporting electrolyte buffer to best simulate the drinking water environment.

2.3.3. Local drinking water sample WOP analysis. The LDW sample analysis was performed without the addition of supporting electrolyte buffers. The same preconditioning of the AuNP-CNTf-CS working electrode by CV and baseline collection by SWASV was done as described in simulated water sample WQP analysis. The six WQPs were studied at an individual working electrode. A 40 mL LDW sample first had 10 µg L^{-1} Pb²⁺ introduced and SWASV was performed in triplicate (n = 3) in the unaltered LDW sample. Then the WQP of interest was adjusted and SWASV measurements were performed in triplicate (n = 3). The SWASV analyses were performed using the same procedure described for the simulated water sample analysis, unless otherwise stated.

2.4. Electrode fabrication and gold modification

The detailed procedures for preparing the CNTf-CS electrode have been described in detail by our group previously. 45,49 First, a CNT fiber was assembled from a vertically aligned MWCNT forest. Then, ~4 cm sections of the CNT fiber were densified in an acetone bath at 30 °C for 96 h. Six densified CNT fibers with diameters of ~70 µm were aligned parallelly and embedded within a polymer in the shape of a 1 cm diameter cylinder. After curing, the embedded CNT fibers were sliced into cross sections with thickness of ~100 μm using a microtome. Fast-drying silver paint was applied to a copper wire and one end of the CNTf-CS to create electrical connections. The silver paint was allowed to dry for one hour before being insulated and secured using 5 min quick setting epoxy. The CNTf-CS microelectrode was used as the bare working electrode. To prepare the modified AuNP-CNTf-CS microelectrode, gold nanoparticles (AuNPs) were electrodeposited onto the CNTf-CS microelectrode using CV (0.2 to -1.6 V, 50 mV s⁻¹, 3 cycles) in 0.5 mM K[AuCl₄] (prepared by ultrasonication for 10 min) with 0.1 M KCl as a supporting electrolyte (SE).

2.5. Optimization of CV cycles for gold modification

The optimal number of CV cycles for AuNP electrodeposition was determined by detecting 10 μg L⁻¹ Pb²⁺ in 0.1 M acetate buffer (pH 4.3) using AuNP-CNTf-CS electrodes prepared using 2, 3, and 5 CV cycles. As shown in Fig. S1,† the electrode prepared using 3 CV cycles exhibited the largest peak height for 10 μ g L⁻¹ Pb²⁺ following the standard SWASV procedure.

3. Results and discussion

Characterization of bare and modified microelectrodes

3.1.1. SEM micrographs. SEM micrographs of the bare and modified AuNP-CNTf-CS electrodes are shown in Fig. 1. The surface morphology of the bare CNTf-CS microelectrode can be seen in Fig. 1A and display the smooth nature of its surface.

Analyst

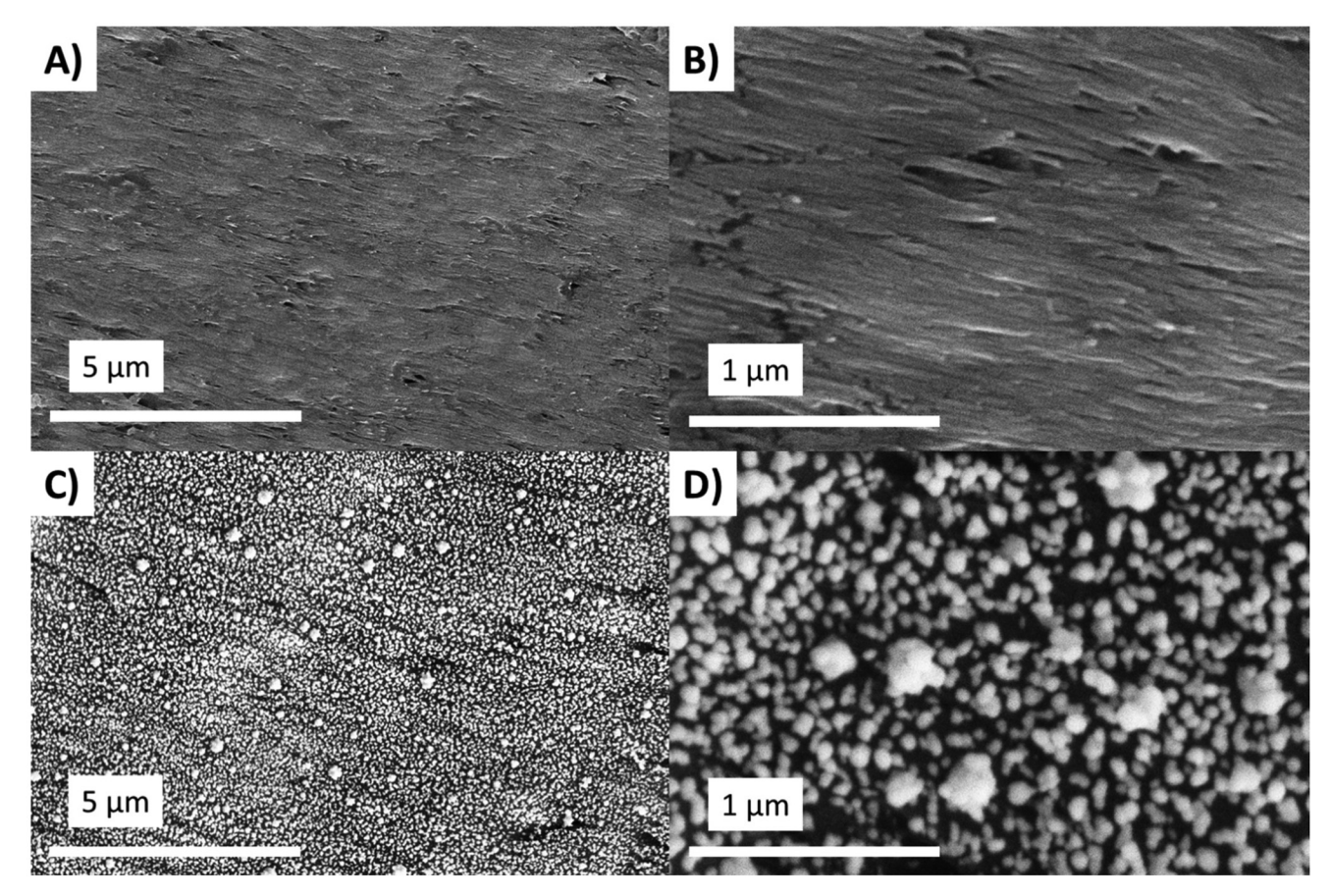


Fig. 1 SEM micrographs of (A and B) the bare CNTf-CS and (C and D) AuNP-CNTf-CS at magnifications of (A and C) 10 000x and (B and D) 50 000×.

The density of the cross section and bundles of MWCNTs can be seen in Fig. 1B and displays the packing density of CNTs. Gold modification resulted in a uniform distribution of AuNPs on the AuNP-CNTf-CS microelectrode surface (Fig. 1C). As shown in Fig. 1D, the AuNPs on the AuNP-CNTf-CS electrode surface were 10-100 nm in diameter, and the bare CNT surface of the electrode was partially exposed. Thus, the bare CNT surface could interact with the electrolyte solution, even after modification with AuNPs.

3.1.2. Raman spectroscopy, EIS, and EDAX. Raman spectroscopy was used to confirm the AuNP deposition on the surface of the CNTf-CS electrode. The presence of metal nanoparticles on a Raman-active substrate results in enhanced Raman intensities due to localized surface plasmon resonance.⁵⁸⁻⁶⁰ The three main Raman peaks (D, G, and G') exhibited enhancement factors of ~14, 18, and 4, respectively (Fig. S2†). The Raman spectroscopy results indicated that the modified AuNP-CNTf-CS electrode was successfully prepared, as discussed further in the ESI.†

EIS data were recorded for the bare CNTf-CS and modified AuNP-CNTf-CS electrodes, and the Nyquist plots are shown in Fig. S3.† As estimated from the diameter of the semicircular feature in the Nyquist plots, the CNTf-CS and AuNP-CNTf-CS electrodes had charge-transfer resistance (R_{ct}) values of approximately 1316 and 589 Ω , respectively. The decrease in Rct for the AuNP-CNTf-CS electrode was attributed to an increase in the geometrical surface area after AuNP modification.

Gold modification was further confirmed using EDAX. The EDAX spectrum of the AuNP-CNTf-CS sample exhibited a large Au peak (Fig. S4B†), whereas this peak was absent from the EDAX spectrum of the bare CNTf-CS sample (Fig. S4A†). Table S2† summarizes the contents (weight %) of selected elements (Au, C, O, Cl, and K) in each sample. The CNTf-CS and AuNP-CNTf-CS samples contained 0.8 and 57.1 wt% gold, respectively, which confirmed that the observed NPs indeed are gold. Elemental identification and weight percentages were analyzed and calculated using TEAM™ eZAF EDS Smart Quant software.

3.1.3. CV characterization. Cyclic voltammograms of 2.5 mM hexaamineruthenium(III) chloride in 0.1 M KCl on the CNTf-CS and AuNP-CNTf-CS electrodes are shown in Fig. S5A.† The peak current response for the redox species was increased on the AuNP-CNTf-CS electrode, which was attributed to the increased surface area of this electrode after modification. Fig. S5B† shows the baseline responses of the CNTf-CS and AuNP-CNTf-CS electrodes in two supporting electrolytes (0.1 M KCl and 0.1 M standard MOPS) with and without nitrogen

bubbling. The onset of the oxygen reduction reaction (ORR) occurred at a potential of approximately -20 mV vs. Ag|AgCl on the AuNP-CNTf-CS electrode, whereas the ORR was not observed on the bare CNTf-CS electrode in 0.1 M KCl solution (Fig. S5B†). Bulk gold and AuNPs have been reported to exhibit catalytic activity for the ORR,61 and the Vodnik group reported an onset potential of -100 mV vs. SCE on an gold polyaniline nanocomposite. 62 Following 5 minutes of nitrogen bubbling, the observed peak was greatly reduced in both the KCl and MOPS solutions (Fig. S5B†) supporting the attribution of the observed peak to ORR. To clearly observe the reduction of hexaamineruthenium(III) chloride to hexaamineruthenium(II) chloride, it was necessary to remove oxygen gas from the hexaamineruthenium(III) chloride solution by purging with nitrogen gas for 30 min (Fig. S5A†).

3.2. Reproducibility and repeatability of the AuNP-CNTf-CS electrode

The reproducibility of the AuNP-CNTf-CS electrode was determined by analyzing five simulated water samples containing 10 μg L⁻¹ Pb²⁺, with three SWASV measurements for each sample on a single electrode (Fig. S6A†). Using the standard SWASV procedure described above, good reproducibility was observed, with a relative error of 5.9%. The repeatability was determined by analyzing simulated drinking water samples containing 10 µg L⁻¹ Pb²⁺ using 5 different AuNP-CNTf-CS electrodes, with 3 SWASV measurements for each sample (Fig. S6B†). Using the standard SWASV procedure described above, the repeatability of the AuNP-CNTf-CS electrode was determined to be 10.4%. Thus, the robustness of the AuNP-CNTf-CS microelectrode was sufficient to ensure confidence in the observed trends for the investigated WQPs.

3.3. Effect of pH on Pb²⁺ detection

The peak height for trace Pb2+ detection in simulated drinking water decreased with increasing pH (Fig. 2A inset). The thermodynamic stabilities of metallic lead, Pb^{2+/4+} ions, and lead compounds in water as a function of pH vs. redox potential have been reported in various Pourbaix diagrams. 28-30,63 Pourbaix diagrams have three zones (immunity, corrosion, and passivation), which are related to the various stable forms of a metal. Lead in acidic water is stable in its soluble divalent ion (Pb²⁺) form, whereas in alkaline water with no other inorganic and organic contaminants, the lead hydroxo cation PbOH⁺ is formed. As the pH increases, the response to Pb2+ ions are decreased by the resulting shift from a corrosive zone to a passivation zone, where Pb2+ ions become less favorable in the equilibrium from Pb²⁺ to PbOH⁺ ions following eqn (1):⁶⁴

$$pH = 6.181 + log \frac{a_{PbOH_{(aq)}}^{+}}{a_{Pb_{af}}^{2+}}$$
 (1)

The SWASV technique relies on a preconcentration step, in which HMIs are reduced electrochemically on the surface of the working electrode. However, based on our results (Fig. 2A) the SWASV technique is less sensitive to PbOH⁺ ions compared to Pb2+ ions. This can also be seen in ESI Fig. S7A† where

plotted is the theoretical concentrations of Pb2+ and PbOH+ with changes in solution pH for a 10 μg L⁻¹ Pb²⁺ sample. For this reason, buffers are typically employed to control the speciation of lead for HMI sensors based on stripping voltammetry.²²

As shown in Fig. 2A, the Pb²⁺ peak in the SWASV curves shifted towards more negative potentials as the pH increased. From pH 6.0 to 8.0, the peak potential shifted by approximately -63 mV. The half-reaction of Pb2+ reduction does not involve hydroxide ions or protons and is not affected by pH, but the half-reaction potential of PbOH⁺ (eqn (2) 64 is pH dependent.

$$E = 0.056 - (0.0295 \times \text{pH}) + 0.0295 \times \log a_{\text{PbOH}_{(ag)}^+}$$
 (2)

The shift in stripping potential from pH 6.0 to 8.0 was experimentally observed to be -63 mV and matches well with the theoretically calculated value of -59 mV. 64 The plot of the experimental and theoretical stripping peak potential shift with pH change is shown in Fig. S7B.† This more negative potential indicates that more energy is required to deposit the PbOH⁺ species and may be the cause of the reduced sensitivity with increasing pH. Changes in working electrode surface energies can also shift stripping potentials,65 which is important when analyzing samples with multiple HMIs, as stripping potentials are used to identify the detected metal species.

The LDW sample data in Fig. 2B had an initial pH value of 9.0 without any alterations and showed an increase in peak height response upon lowering the pH to 6.9. The decrease was less substantial than observed in the simulated water sample. We attribute this to the complexity of the typical drinking water sample. The shift in stripping peak potential was not observed indicating that we are not observing the same Pb²⁺/PbOH⁺ equilibrium. The LDW sample had a CaCO₃ concentration of 133 mg L⁻¹ which will affect the lead speciation expected from the lead Pourbaix diagram. This indicates that pH has less of an effect on the SWASV technique in the LDW sample tested. Ideally, the SWASV technique should be performed after sample acidification to ensure that all lead species are in the Pb2+ ion form, although this is not always possible. Nevertheless, using SWASV, we were still able to detect trace lead at the alkaline pH value of 8.0 in the simulated water sample. Source waters used for municipal drinking water typically have pH values in the range of 6.5-8.5, but they can be higher or lower depending on the environment.³² The detection of trace heavy metals using SWASV becomes more challenging at more alkaline pH values, as evidenced by the thermodynamic stability of lead in Pourbaix diagrams, our SWASV results in Fig. 2A, and HMI sensor research. 22,23,66 As shown in the LDW sample (Fig. 2B) the change in pH played a much smaller role in the effect of peak potential and height. Observing a prominent peak at pH value of 9.0 in the LDW sample reveals the use of this technique does not require pH adjustment by buffers for trace detection of lead.

Analyst Paper

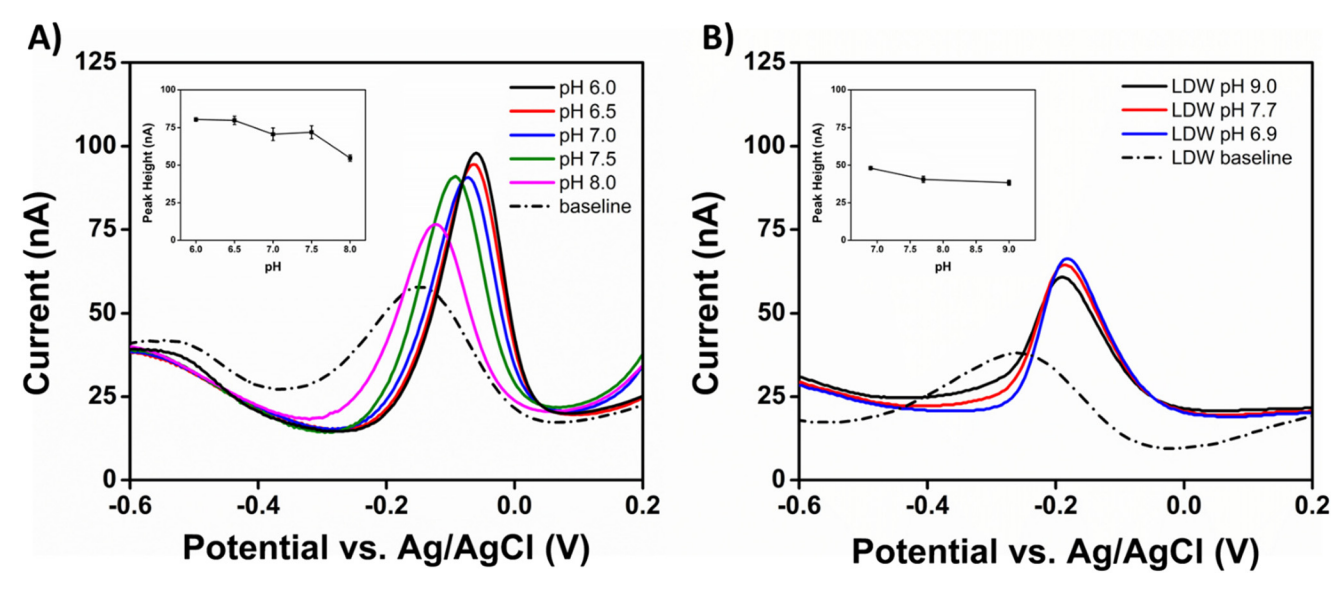


Fig. 2 (A) Simulated water sample SWASV analysis on the AuNP-CNTf-CS electrode containing 10 μ g L⁻¹ Pb²⁺ at pH values of 6.0, 6.5, 7.0, 7.5, and 8.0. (B) LDW sample SWASV analysis on the AuNP-CNTf-CS electrode containing 10 μ g L⁻¹ Pb²⁺ at unaltered pH value of 9.0, and adjusted pH values 7.7 and 6.9. Insets of (A) and (B) shows the peak heights at the different pH values with error bars (n = 3). The dotted curves in (A) and (B) shows the baseline before addition of 10 μ g L⁻¹ Pb²⁺.

3.4. Effect of conductivity on Pb²⁺ detection

The conductivity of a solution is a crucial factor in electrochemistry for allowing charge transfer between two polarized electrodes in an electrochemical cell. We observed an increase in the peak height for trace Pb²⁺ detection in simulated drinking water as the conductivity increased (Fig. 3A). During the stripping step of SWASV, electrons are transferred to and from

the electrode and solution and charged ions migrate between the electrodes for charge compensation. Thus, a SE is added to electrochemical cells to maintain electrical neutrality via charge transfer in solution. Solutions with low conductivities or insufficient amounts of SE can experience ohmic drop. Ohmic drop describes the solution resistance (R_s) between the working and counter electrodes, which can behave as a true resistor in an electrochemical cell over a wide range of con-

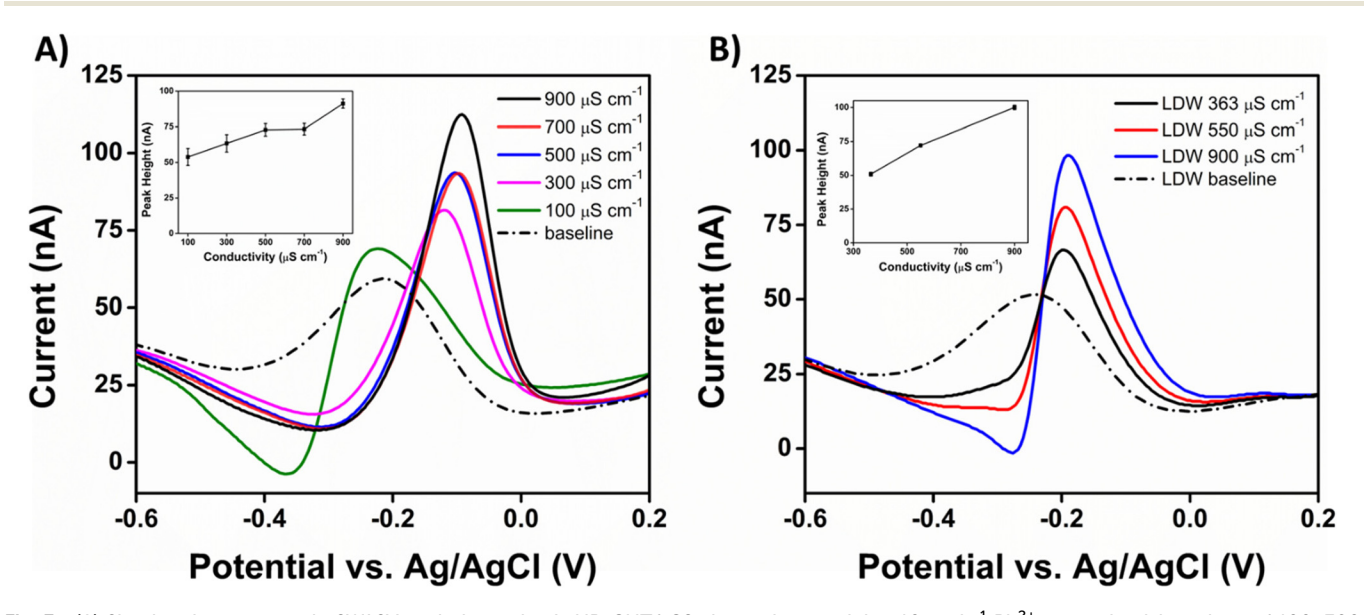


Fig. 3 (A) Simulated water sample SWASV analysis on the AuNP-CNTf-CS electrode containing 10 μ g L⁻¹ Pb²⁺ at conductivity values of 100, 300, 500, 700, and 900 μ S cm⁻¹. (B) LDW sample SWASV analysis on the AuNP-CNTf-CS electrode containing 10 μ g L⁻¹ Pb²⁺ at unaltered conductivity value of 363 μ S cm⁻¹, and adjusted conductivity values 550, and 900 μ S cm⁻¹. Insets of (A) and (B) shows the peak heights at the different conductivity values with error bars (n = 3). The dotted curves in (A) and (B) shows the baseline before addition of 10 μ g L⁻¹ Pb²⁺.

ditions. Ohmic drop can cause a polarized electrode to experience a lower potential than that recorded and applied by the electrochemical workstation.^{39,65,67} This phenomenon can cause artificial peak potential shifting as well as peak distortion and slower electron transfer kinetics. The potential experienced at the working electrode can be represented by eqn (3):⁶⁵

$$E_{\text{appl}} = E_{\text{eq,Pb}} + \eta - iR_{\text{s}} \tag{3}$$

where E_{appl} is the applied potential controlled by the potentiostat, $E_{\text{eq.Pb}}$ is the standard reduction potential of Pb²⁺, η is the overpotential needed to support the electrochemical reaction rate corresponding to the current (i), and R_s is the solution resistance. The magnitude of the current measured due to the reduction and oxidation of Pb²⁺ depends on the η applied at the working electrode. As R_s increases, the E_{appl} must increase proportionally to achieve the same current at the working electrode. During the stripping step of SWASV, preconcentrated lead is repeatedly oxidized and re-reduced at the electrode surface due to the pulsing of the potential at a frequency of 15 Hz. As the applied potential at the working electrode decreases, the current produced during each of these pulses decreases. As a result, in our SWASV measurements the Pb²⁺ peak decreased as the conductivity of the simulated water samples decreased (Fig. 3A).

The voltammogram of the simulated water sample with the lowest conductivity (100 μS cm $^{-1}$) exhibited a distorted peak (Fig. 3A), likely because the polarization of the working electrode during the stripping step changed more slowly than the frequency of the pulsing potential. If the potential experienced at the working electrode cannot keep up with the instrument's commands, the instrument will record current responses at potentials that are not being experienced by the working electrode. The distorted peak at approximately -215 mV observed for the simulated water sample with a conductivity of 100 μS cm $^{-1}$ complicates the voltammogram interpretation and may cause peaks to merge and further distort in the presence of other HMIs. Thus, if a water sample has insufficient conductivity, adjustments should be made before SWASV analysis.

The real drinking water sample had a conductivity of $363~\mu S~cm^{-1}$ without any alterations and was adjusted to $550~and~900~\mu S~cm^{-1}$ to explore the effect of conductivity in a complex sample. The SWASV voltammograms in Fig. 3B showed an increased in peak height response with increasing conductivity. The magnitude of the peak height increase is comparable between the simulated water sample and the LDW sample shown in the insets of Fig. 3A and B. The conductivity remains a vital WQP for the SWASV technique even in a more complex water sample.

Electrochemical cells can be modified to accommodate high resistance solutions by placing the working and reference electrodes close together, using microelectrodes to decrease the current, and adding a SE to increase the conductivity. Modern instrumentation has circuitry designed to compensate for the resistance of the solution using positive feedback compensation schemes. Optimization of the SWASV technique's parameters such as frequency, amplitude and potential step may provide clear voltammograms without the need for increasing solution conductivity. The quantitative and qualitative detection of trace Pb^{2+} in simulated drinking water using the SWASV technique with the AuNP-CNTf-CS microelectrode required a sufficient conductivity of more than 100 μ S cm⁻¹.

3.5. Effect of free chlorine on Pb²⁺ detection

To study the effect of free chlorine on Pb²⁺ detection in simulated water samples, we used NaClO concentrations of 1.0, 2.0, 3.0, and 4.0 mg L⁻¹, which are representative of the range allowed in drinking water by the US EPA. The sensitivity of the SWASV technique to trace Pb²⁺ decreased as the amount of free chlorine was increased (Fig. 4A).

In solution, NaClO hydrolyzes to form hypochlorous acid (HClO), as shown in eqn (4):

$$NaClO + H_2O \rightarrow Na^+ + HClO + OH^-$$
 (4)

HClO is a weak acid that dissociates *via* a pH-dependent equilibrium following eqn (5):

$$HClO \rightleftharpoons H^+ ClO^-$$
 (5)

The active chemical species formed by primary chlorine disinfectants, commonly referred to as "free" or "available" chlorine, are in the form of either HClO or the hypochlorite ion (ClO⁻). The equilibrium between these species is pH dependent, with ~80% HClO and ~20% ClO occurring at pH 7.0. Thus, HClO is expected to be the prevalent species in our simulated chlorine drinking water samples. 68 The ClO- hypochlorite ion is a strong oxidizing agent and can oxidize Pb2+ to Pb⁴⁺ which is unstable and will precipitate forming insoluble PbO₂.²⁹ The SWASV technique is blind to PbO₂ precipitates thus showing the decrease in peak height at higher free chlorine levels. It is clear that not all the Pb2+ was oxidized as a peak can still be observed after 4 mg L⁻¹ of NaOCl was added to the solution. Further addition of NaOCl from 3 to 4 mg L⁻¹ showed negligible change in the peak height in Fig. 4A inset. Even at the highest allowable free chlorine concentration there are still detectable lead species by the SWASV technique in solution.

The LDW sample contained 0.45 mg L^{-1} free chlorine without any alterations and was adjusted to 2.0 and 4.0 mg L^{-1} to study its effect in a complex water sample. Fig. 4B shows the voltammograms of 10 μ g L^{-1} Pb²⁺ with increasing free chlorine concentrations. The results show a decrease in peak height response (Fig. 4B inset) similar to the simulated water study. In the LDW sample a shift in peak shape and potential are observed which was not seen in the simulated water samples. At the pH value of 9.0 in the LDW sample the equilibrium shifts to ~10% HClO and ~90% ClO $^-$, providing more of the oxidizing species. With a higher presence of the oxidizing agent ClO $^-$ it likely to cause a change in the lead species more substantially than in the simulated water with a pH of 7.0. This results in the voltammograms lead peak broadening and

Analyst Paper

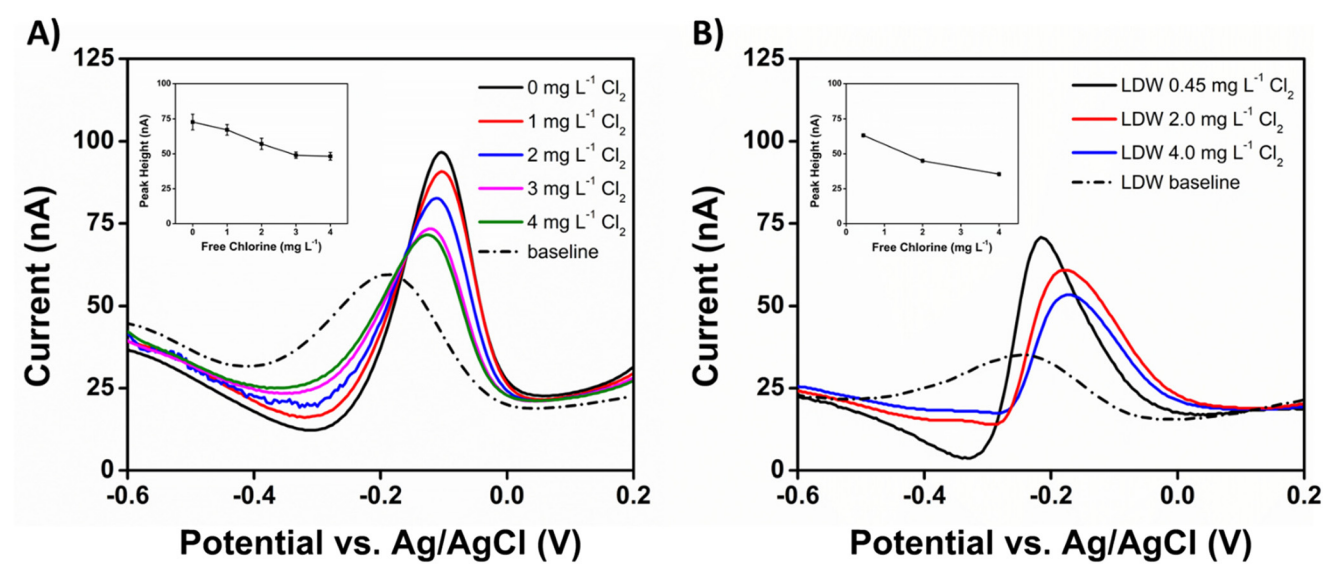


Fig. 4 (A) Simulated water sample SWASV analysis on the AuNP-CNTf-CS electrode containing 10 μ g L⁻¹ Pb²⁺ and 0.0, 1.0, 2.0, 3.0, and 4.0 mg L⁻¹ NaClO. (B) LDW sample SWASV analysis on the AuNP-CNTf-CS electrode containing 10 μg L⁻¹ Pb²⁺ at unaltered free chlorine value of 0.45 mg L⁻¹ NaClO, and adjusted free chlorine concentrations of 2.0, and 4.0 mg L⁻¹ NaClO. Insets of (A) and (B) shows the peak heights at the different free chlorine concentrations with error bars (n = 3). The dotted curves in (A) and (B) shows the baseline before addition of 10 ug L⁻¹ Pb²⁺.

stripping potential shifting to a more positive potential. Further research on the mechanism of the oxidation of Pb2+ to Pb⁴⁺ and its subsequent precipitation to PbO₂ is needed to better understand lead speciation formed in solution in the presence of ClO-. It can be expected that high pH values will increase the effect of free chlorine on the SWASV technique for lead detection. The speciation of lead can be affected by free chlorine. Cantor et al. reported that chlorine species influence lead solubility by oxidizing Pb2+ to Pb4+, which can precipitate as insoluble lead(IV) oxide (PbO2).29 In addition, Cantor et al. evaluated the effect of chlorine on the corrosion of lead piping by drinking water samples and found less lead in the effluent water with added chlorine than in untreated drinking water.²⁹ Our results also suggest a decrease in Pb²⁺ solubility as the free chlorine concentrations in our simulated drinking water increased. At higher free chlorine concentrations, the sensitivity of the SWASV technique is decreased shown in both the simulated and LDW samples. The amount and chemicals used to introduce free chlorine by the WWS can be found in their annual reports, and this information can be used before water to predict if the levels will be high enough to effect detection of lead by the SWASV technique. At higher levels of free chlorine and high pH values it can be expected that the lead peak will be decrease and possibly broadened compared to a water sample without free chlorine.

3.6. Effect of alkalinity (HCO₃⁻) on Pb²⁺ detection

Increasing the alkalinity initially decreased the peak height response of the SWASV technique for trace Pb2+ detection in simulated drinking water, but CaCO3 concentrations above 50 mg L⁻¹ had little effect on the response (Fig. 5A inset). Boyd et al. calculated the maximum solubility of CaCO3 in water to

be 7.1 mg L⁻¹ from its solubility constant in water at neutral pH.³⁴ However, in natural water systems, limestone, which mainly consists of CaCO₃, can be dissolved in larger amounts than predicted due to dissolved CO2. Surface water contains dissolved CO2 in equilibrium with the atmosphere, which affects the form of carbonate species. CO2 will react with water to form carbonic acid (H₂CO₃) in very small amounts.^{34,37} Moreover, CaCO3 in the presence of dissolved carbon dioxide (CO₂) will form HCO₃⁻, as shown in eqn (6):

$$CaCO_3 + CO_2 + H_2O \rightarrow Ca(HCO_3)_2$$
 (6)

As CO2 is consumed during the hydrolysis of CaCO3, more CO₂ must be dissolved in water for the system to re-equilibrate. The presence of dissolved CO₂ in water and its effect on the solubility of CaCO3 indicates that CaCO3 in drinking water is present in the form of Ca²⁺ and HCO₃⁻. Therefore, to adjust the alkalinity of the simulated water solutions, CaCO₃ was dissolved by bubbling with CO₂(g) for 30 min with stirring.

Although the sorption of lead onto lead carbonate substrates has been studied for the treatment and prevention of lead contaminated waters, 30,69 there are many discrepancies in the thermodynamic stabilities of the various lead carbonate scales formed inside water pipes. 30 The observed decrease in sensitivity for trace Pb2+ detection at high alkalinity was attributed to the reaction of Pb2+ ions with HCO3- ions in water at neutral pH to form insoluble lead carbonate (PbCO₃) as shown in eqn (7):

$$Pb^{2+} + 2HCO_3^- \to PbCO_3 + H_2O$$
 (7)

The voltammograms in Fig. 5A collected during the alkalinity study agreed with the thermodynamic predictions that insoluble PbCO₃ is formed upon the addition of HCO₃⁻(aq).

Published on 30 June 2022. Downloaded by UNIVERSITY OF CINCINNATI on 7/8/2022 2:03:49 PM.

Paper Analyst

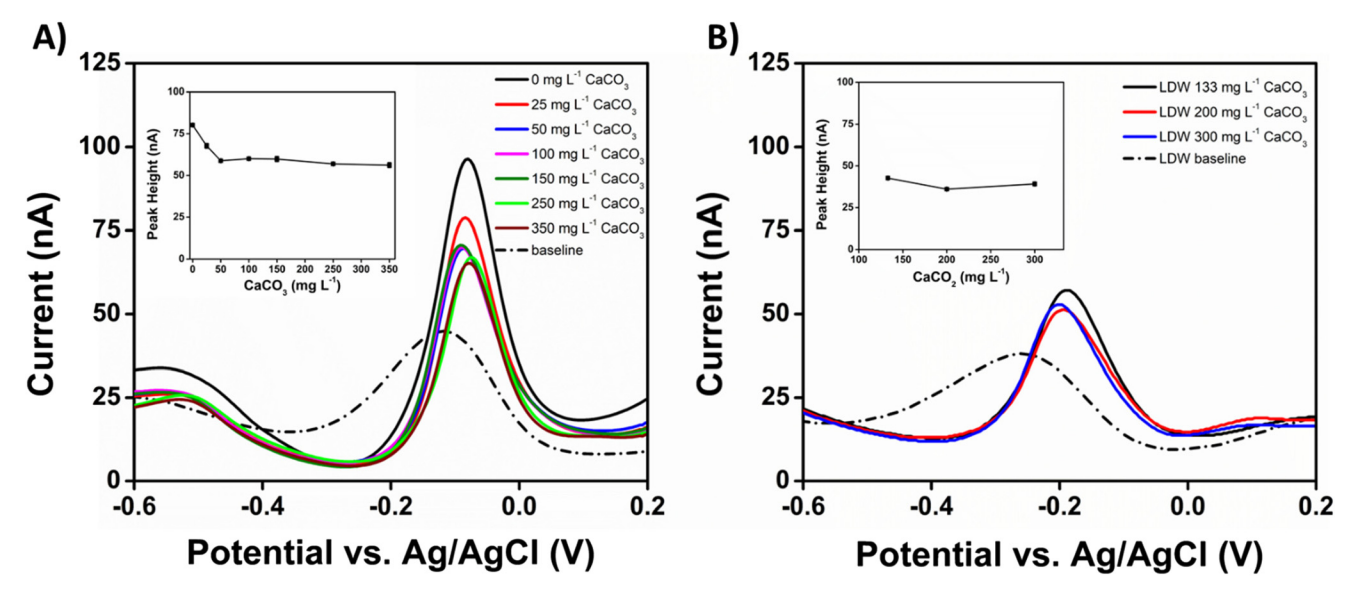


Fig. 5 (A) Simulated water sample SWASV analysis on the AuNP-CNTf-CS electrode containing 10 µg L⁻¹ Pb²⁺ and 0, 50, 100, 150, 250, 300, and 350 mg L^{-1} CaCO₃. (B) LDW sample SWASV analysis on the AuNP-CNTf-CS electrode containing 10 μ g L^{-1} Pb²⁺ at unaltered alkalinity concentration of 133 mg L⁻¹ CaCO₃, and adjusted alkalinity concentrations of 200, and 300 mg L⁻¹ CaCO₃. Insets of (A) and (B) shows the peak heights at the different alkalinity concentrations with error bars (n = 3). The dotted curves in (A) and (B) shows the baseline before addition of 10 μ g L⁻¹ Pb²⁺.

The peak height did not change significantly after the addition of 50 mg L⁻¹ CaCO₃, suggesting that equilibrium was reached.

The LDW sample had an alkalinity of 133 mg L⁻¹ CaCO₃ without any alterations and was increased to 200 and 300 mg L⁻¹ CaCO₃ to study the effect in a complex sample. In Fig. 5B the voltammograms had a peak height percent change of -15.5% from 133 to 200 mg L⁻¹ CaCO₃. The peak heights plotted in the inset of Fig. 5B show the changes in currents (Fig. S6A†). These changes in peak height with alkalinity above 100 mg L⁻¹ CaCO₃ are much less substantial compared with changes observed in the other WQPs, especially the conductivity study having a peak height change of 41.6% from 363 µS cm⁻¹ to 550 µS cm⁻¹. It can be reasoned that water samples with alkalinity levels over 100 mg L⁻¹ CaCO₃ will have suppressed peak heights compared those with 0 mg L⁻¹ CaCO₃ but further increases in alkalinity will have little effect the peak response. The response to alkalinity did not seem to be greatly affected by the complexity of the LDW sample, having similar trends to that observed in the simulated water sample.

The effect of CaCO3 is a reduction in peak height up to approximately 100 mg L⁻¹ where further increases will have little effect on peak response. Researchers analyzing various water samples should only be concerned with fluctuations of a water samples alkalinity if it is changing in the range of 0-100 mg L⁻¹ as these shifts in peak heights can be large. At high alkalinities even up to 300 mg L⁻¹ a prominent peak for trace lead levels is clearly observed in simulated and the LDW sample.

3.7. Effect of temperature on Pb²⁺ detection

The temperature of drinking water varies as it moves through a water distribution system and upon entry into premise plumb-

ing. The temperature of drinking water can be affected by the season, water source, premise plumbing environment, and hot water heaters and boilers. 42 As shown in Fig. 6A, the peak height response of the SWASV technique towards Pb2+ was increased with increasing temperature. Many insoluble lead species exhibit limited solubility at high temperatures, which may have a small influence on Pb²⁺ detection. In particular, as the temperature increases, (Pb(OH)₂) precipitates can be dissolved at pH 7.0.43

The ionic conductivity of a solution increases as the temperature increases, owing to the influence of temperature on the mobility of ions and the dissociation of ionizable species in solution.⁷⁰ Shown in the conductivity study performed in both simulated and LDW samples was also an increase in peak height (Fig. 3A and B). The activity of both the ions providing solution conductivity as well as the activity of the Pb2+ is proportional to the temperature.⁷¹

The ability of the SWASV technique to detect Pb2+ ions at low temperatures was greatly hindered, as the peak response at 10 °C was similar to the baseline response (Fig. 6A). However, in the presence of Pb2+ ions, the peak appeared at approximately -129 mV, whereas the baseline response peak was observed at approximately -179 mV. This difference in peak potentials allowed for the interpretation of the SWASV response to trace Pb2+ at low temperatures. This baseline characteristic peak is attributed to the oxidation and reduction of functional hydroxyl and carboxyl groups known to be present at the CNT surface and once interacted with Pb2+ they become unreactive.

The LDW sample was tested at 10, 23, and 30 °C to study the effect of temperature in a complex sample. Fig. 6B the peak height response is greatly enhanced with the increase in

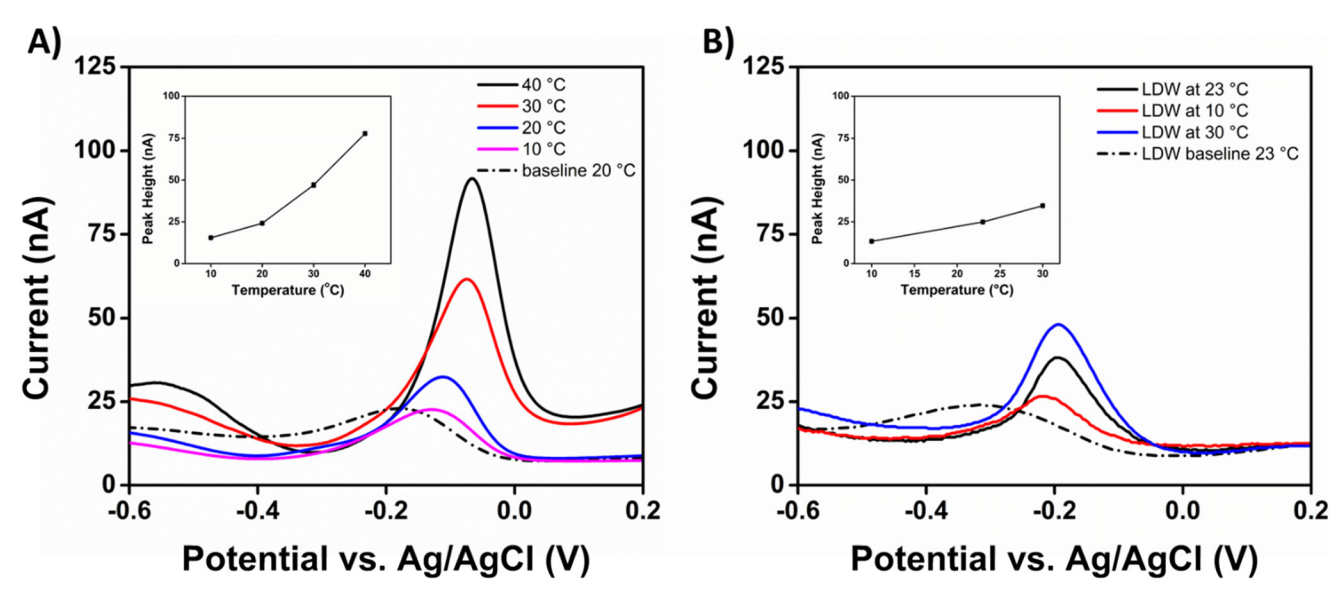


Fig. 6 (A) Simulated water sample SWASV analysis on the AuNP-CNTf-CS electrode containing 10 μ g L⁻¹ Pb²⁺ at temperatures 10, 20, 30, and 40 °C. (B) LDW sample SWASV analysis on the AuNP-CNTf-CS electrode containing 10 μ g L⁻¹ Pb²⁺ in unaltered water sample at temperatures 10, 23, and 30 °C. Insets of (A) and (B) shows the peak heights at the different temperatures with error bars (n = 3). The dotted curves in (A) and (B) shows the baseline before addition of 10 μ g L⁻¹ Pb²⁺.

temperature from 23 to 30 $^{\circ}$ C and substantially decreased at 10 $^{\circ}$ C. The response in the LDW sample reveals the same expected results as in simulated water, as the increase in solution conductivity with temperature will produce increasing of peak intensities.

Increasing the temperature of drinking water before SWASV analysis will increase the sensitivity to Pb²⁺. Ultimately, as the sensitivity of the SWASV technique to Pb²⁺ ions is greatly influenced by temperature, during SWASV calibration, it is critical that the temperature is controlled to match that of the water sample of interest.

3.8. Effect of copper on Pb²⁺ detection

As a common interferent, copper can affect Pb^{2+} detection using the SWASV technique. Our group has previously reported a 50% decrease in the peak response on an inkjet-printed CNT electrode at low Pb^{2+} concentrations with the addition of only $10~\mu g~L^{-1}~Cu^{2+}.^{24}$ Copper can compete for electrode active sites during the deposition step, shift the stripping potential, cause shoulders to appear on peaks, and distort peak shape, thus decreasing the sensitivity towards Pb^{2+} ion detection. Pb^{2+}

In Fig. 7A inset the peak heights of 10 μ g L⁻¹ Pb²⁺ using the SWASV technique in the simulated water sample decreased as the Cu²⁺ concentration was increased. Fig. 7A SWASV voltammograms exhibited two separate Pb²⁺ peaks at potentials –150 and –409 mV labeled Pb-1 and Pb-2, respectively. The copper stripping peak appeared prominently at +230 mV labeled Cu-1 in Fig. 7A. In the presence of trace Cu²⁺ (10 μ g L⁻¹) the height of the Pb-1 peak decreased by 25%. This peak was further decreased by 92% with the addition of 100 μ g L⁻¹ Cu²⁺ and was no longer distinguishable at Cu²⁺ concentrations at 200 μ g L⁻¹. The decrease in peak height is attributed to competition

for the AuNP-CNTf-CS electrode's active sites, and as the Cu2+ is deposited it leaves fewer free site for Pb²⁺ deposition. The peak potential is observed to be continually shifted more negative indicating that the Pb2+ is being deposited as a copperlead intermetallic compound. The Cu-1 peak does not increase after 100 μ g L⁻¹ Cu²⁺ and the Pb-1 peak at -150 mV grows as broad distorted peak due to the copper-lead intermetallic interactions. The Pb-2 peak appeared after the addition of 50 μ g L⁻¹ Cu²⁺ (Fig. 7A) and did not increase substantially from 100 to 200 μ g L⁻¹ Cu²⁺. Indicating that this Pb-2 peak is due Pb2+ being reduced without forming an intermetallic compound with copper, attributed to Pb²⁺ deposition at the bare CNT surface exposed. With the increase of Cu²⁺ concentrations the broad intermetallic peak at approximately -50 mV continued to grow, and the Cu-1 peak was not increased but broadened and shifted negative. Copper and lead have a high interaction during SWASV analysis and can greatly distort peak shapes, and potentials. When analyzing water samples, a calibration curve of simultaneously detecting Pb and Cu would be recommended to clearly interpret voltammograms with both metals are known to be present in solution.

The individual and simultaneous peaks of Pb^{2+} and Cu^{2+} were explored at high concentrations (20 mg L^{-1}) using CV (+300 to -800 mV, 50 mV s⁻¹) in the standard simulated water solution (0.1 M MOPS, pH = 7.0, conductivity = $500 \ \mu S \ cm^{-1}$) (Fig. S8†). During the forward negative potential scan of 20 mg L^{-1} Pb^{2+} , three separate cathodic peaks (C_{Pb-1} , C_{Pb-2} , and C_{Pb-3}) were observed in the cyclic voltammogram at approximately -89, -354, and -579 mV, respectively (Fig. S8C†). During the reverse positive potential scan, three anodic peaks (A_{Pb-1} , A_{Pb-2} , and A_{Pb-3}) were observed at approximately -377, -252, and -218 mV, respectively. The C_{Pb-1} peak was located at a more

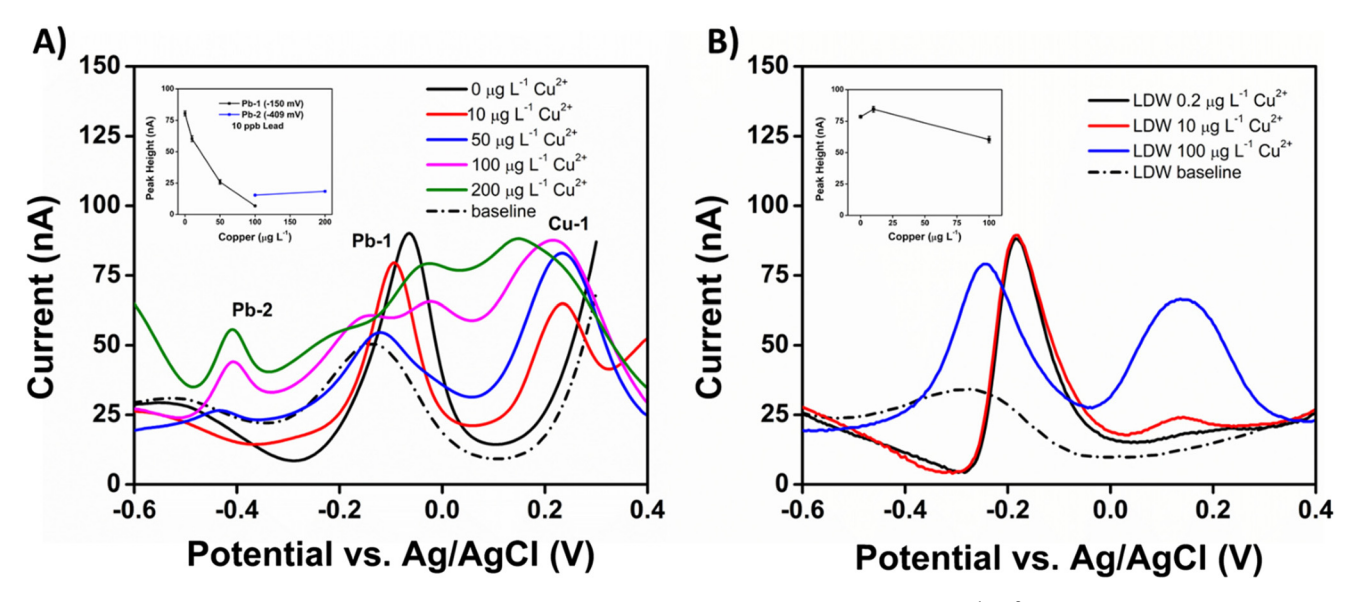


Fig. 7 (A) Simulated water sample SWASV analysis on the AuNP-CNTf-CS electrode containing 10 μ g L⁻¹ Pb²⁺ and 0, 10, 50, 100, and 200 μ g L⁻¹ Cu^{2+} . (B) LDW sample SWASV analysis on the AuNP-CNTf-CS electrode containing 10 μ g L^{-1} Pb²⁺ at unaltered copper concentration of 0.2 μ g L^{-1} Cu²⁺, and adjusted copper concentrations of 10 and 100 µg L⁻¹ Cu²⁺. Insets of (A) and (B) shows the peak heights at the different copper concentrations with error bars (n = 3). The dotted curves in (A) and (B) shows the baseline before addition of 10 μ g L⁻¹ Pb²⁺.

oxidizing (positive) potential than the A_{Pb-1} peak, which indicated that the UPD phenomenon occurred on the AuNP-CNTf-CS electrode during Pb²⁺ reduction.^{54,73} The UPD phenomenon also occurred on the AuNP-CNTf-CS electrode during Cu^{2^+} reduction, as the cathodic peaks (C_{Cu-1}, C_{Cu-2}, and C_{Cu-3}) in the cyclic voltammogram of 20 mg L⁻¹ Cu²⁺ appeared at approximately +163, -84, and -551 mV, respectively (Fig. S8A and S8B†), whereas the anodic peaks $(A_{Cu-1+2}$ and $A_{Cu-3})$ occurred at approximately +62 and -639 mV respectively (Fig. S8A and S8C†). Fig. S8D† shows how the simultaneous presence of 20 mg L⁻¹ Cu²⁺ and Pb²⁺ affected the redox peaks. The cathodic UDP peak CPb-1 was not observed at high Cu2+ concentration owing to the formation of a copper monolayer on the surface of AuNPs, as indicated by presence of the cathodic UPD peak C_{Cu-1}. The bulk deposition of Pb²⁺ still occurred as revealed by the presence of the cathodic peaks C_{Pb-2}, and C_{Pb-3}, although the corresponding Pb²⁺ oxidation peaks were greatly reduced in the presence of 20 mg L⁻¹ Cu²⁺. The deposition of Pb²⁺ is expected to be deposited during SWASV by the UDP phenomena forming a monolayer on the gold nanoparticles and this can be influenced by the presence of another deposited metal ion in solution as seen with Cu²⁺ causing multi-layer formations as well as metal-metal deposition. This is observed in the shift in lead stripping peak potential upon the addition of small Cu²⁺ concentrations and then a completely new stripping potential forming at higher Cu²⁺ concentrations. These peak shifting characteristics are attributed to Pb2+ starting to compete for deposition on the gold nanoparticles as a monolayer, followed by metal-metal multilayers forming shifting peak potential and finally starts depositing on the bare CNT surface completely moving the stripping peak potential.

The LDW collected had an initial copper concentration of only 0.22 $\mu g L^{-1} Cu^{2+}$ and was increased to 10 and 100 $\mu g L^{-1}$ Cu²⁺ to further understand the interference copper has on Pb²⁺ detection in a complex sample. Fig. 7B SWASV voltammograms in the LDW sample had a much different response to increasing Cu²⁺ concentrations than observed in the simulated water sample. At the addition of 10 μ g L⁻¹ Cu²⁺ a peak is observed at +135 mV with a peak height of only 7.5 nA compared to the 31.4 nA peak height observed in the simulated water. The Pb²⁺ peak with 10 μg L⁻¹ Cu²⁺ is not decreased as observed in the simulated water sample. This is due to Cu²⁺ precipitating through hydrolysis to insoluble Cu(OH)2 at pH of 9.0, and at pH of 7.0 the Cu²⁺ species is more prevalent.⁷⁴ As the Cu²⁺ is increased to 100 µg L⁻¹ the copper peak grows at the same potential (+135 mV) and the lead peak height is decreased and shifted more negative, as observed in the simulated water samples. The increased pH causes less soluble copper to be present in solution and greatly diminishes its effect on the Pb2+ deposition until greater copper concentrations are added.

The copper interference observed is diminished at high pH values due to the hydrolysis of Cu²⁺ to Cu(OH)₂ which will not deposited on the working electrode surface during SWASV analysis. At low pH values the effect of even trace copper concentrations is a decrease in peak height response and stripping peak potential shifting. The mechanism of copper-lead intermetallic interactions at the working electrode surface demands further research to understand the interactions observed here. The study of Cu²⁺ detection using SWASV in various pH solutions is also needed to better predict the influence copper's presence will have on the SWASV detection of trace Pb²⁺.

4. Conclusion

We report six WQPs and their influence on the SWASV technique for detecting trace Pb2+ ions. Each of the investigated WQPs (pH, conductivity, chlorine, alkalinity, temperature, and copper) had a different effect on the SWASV technique for Pb²⁺ detection. The parameters were explored in both simulated water samples and drinking water samples. In the simulated water samples the peak heights of trace Pb2+ detection by SWASV was proportional with conductivity, and temperature and inversely proportional with pH, free chlorine, alkalinity, and copper. The applicability of these results was confirmed in real drinking water samples, showing the same relationship between lead detection and the WOPs tested. The pH in the drinking water sample had much lower increase of peak height at lower pH values due to the alkalinity of the solution. The free chlorine's oxidizing species equilibrium can shift with pH, and we observed that free chlorine had a larger (negative) effect at higher pH values. The copper species present in solution is pH dependent with larger Cu²⁺ ion concentration at lower pH values. At higher pH values copper had a substantially decreased (negative) effect on the SWASV analysis of Pb²⁺. The two parameters that had the largest impact on Pb²⁺ detection by SWASV were conductivity and copper levels. The conductivity showed the greatest increase in peak height in the range studied and at the lowest conductivity tested the Pb²⁺ stripping peak was distorted making interpretation of the voltammogram challenging. The copper interfered with the Pb²⁺ peak height at trace levels causing large shifts in stripping peak potential. Using the SWASV technique the detection of 10 μg L⁻¹ Pb²⁺ was accomplished even at the worst-case scenarios for each simulated WQP. By considering the sample preparation conditions, the applicability of the SWASV technique to Pb2+ ion detection in drinking water samples can be improved without requiring SE or buffer addition.

Conflicts of interest

The authors declare no competing financial interest.

Acknowledgements

The authors are indebted to professorship start-up funds from the Department of Chemistry at the University of Cincinnati, NSF 2016484 PFI grant and Prof Shanov for providing the CNT fibers.

Notes and references

1 K. J. Pieper, R. Martin, M. Tang, L. Walters, J. Parks, S. Roy, C. Devine and M. A. Edwards, Evaluating water lead levels during the flint water crisis, *Environ. Sci. Technol.*, 2018, 52(15), 8124–8132, DOI: 10.1021/acs.est.8b00791.

- 3 W. L. Lee, J. Jia and Y. Bao, Identifying the gaps in practice for combating lead in drinking water in Hong Kong, *Int. J. Environ. Res. Public Health*, 2016, **13**, 1–18, DOI: **10**.3390/ijerph13100970.
- 4 S. Chowdhury, F. Kabir, M. A. J. Mazumder and M. H. Zahir, Modeling lead concentration in drinking water of residential plumbing pipes and hot water tanks, *Sci. Total Environ.*, 2018, 635, 35–44, DOI: 10.1016/j. scitotenv.2018.04.065.
- 5 D. K. Roth, J. R. Wagner and D. A. Cornwell, Impacts of source water blending on lead release, *J. Am. Water Works Assoc.*, 2018, **110**, 15–25, DOI: **10.1002/awwa.1129**.
- 6 K. J. Pieper, M. Tang and M. A. Edwards, Flint water crisis caused by interrupted corrosion control: investigating "ground zero" home, *Environ. Sci. Technol.*, 2017, 51, 2007–2014, DOI: 10.1021/acs.est.6b04034.
- 7 D. A. Lytle, M. R. Schock, K. Wait, K. Cahalan, V. Bosscher, A. Porter and M. Del Toral, Sequential drinking water sampling as a tool for evaluating lead in flint, Michigan, *Water Res.*, 2019, 157, 40–54, DOI: 10.1016/j. watres.2019.03.042.
- 8 M. R. Lasheen, C. M. Sharaby, N. G. El-Kholy, I. Y. Elsherif and S. T. El-Wakeel, Factors influencing lead and iron release from some Egyptian drinking water pipes, *J. Hazard. Mater.*, 2008, **160**, 675–680, DOI: **10.1016/j.** jhazmat.2008.03.040.
- 9 S. Martin and W. Griswold, *Human health effects of heavy metals*, Cent. Hazard. Subst., 2009, pp. 1–6.
- 10 Z. Rahman and V. P. Singh, The relative impact of toxic heavy metals (THMs) (arsenic (As), cadmium (Cd), chromium (Cr)(v1), mercury (Hg), and lead (Pb)) on the total environment: an overview, *Environ. Monit. Assess.*, 2019, 191(7), 419, DOI: 10.1007/s10661-019-7528-7.
- 11 I. Thornton, R. Rautiu and S. M. Brush, *Lead the facts*, IC Consultants Ltd, London, UK, 2001.
- 12 H. Needleman, Lead Poisoning, *Annu. Rev. Med.*, 2003, 55, 209–222, DOI: 10.1146/annurev.med.55.091902.103653.
- 13 M. Jaishankar, T. Tseten, N. Anbalagan, B. B. Mathew and K. N. Beeregowda, Toxicity, mechanism and health effects of some heavy metals, *Interdiscip. Toxicol.*, 2014, 7, 60–72, DOI: 10.2478/intox-2014-0009.
- 14 W. M. Haschek, C. G. Rousseaux and M. A. Wallig, *Haschek and Rousseaux's handbook of toxicologic pathology*, Elsevier, 2013, DOI: 10.1016/C2010-1-67850-9.
- 15 R. L. Boeckx, Lead poisoning in children, *Anal. Chem.*, 1986, 58(2), 274A–288A, DOI: 10.1021/ac00293a001.
- 16 US EPA, 2018 Edition of the drinking water standards and health advisories, Off. Water U.S. Environ. Prot. Agency, Washington, DC, 2018, pp. 1–20. DOI: EPA 822-S-12-001.
- 17 World Health Organization (WHO), Lead in drinking-water: background document for development of WHO guidelines fro drinking-water quality, *World Health Organization*, 2013, 2, 1–16, https://apps.who.int/iris/handle/10665/75370.

Paper

18 IIS FDA National primary drinking water regulations for lead Works Assoc 2000

- 18 US EPA, National primary drinking water regulations for lead and copper: short-term regulatory revisions and clarifications, final rule, Fed. Regist., 2007, vol. 72, pp. 1–40.
- 19 C. K. de Andrade, P. M. K. de Brito, V. E. dos Anjos and S. P. Quináia, Determination of Cu, Cd, Pb and Cr in yogurt by slurry sampling electrothermal atomic absorption spectrometry: A case study for Brazilian yogurt, *Food Chem.*, 2018, 240, 268–274, DOI: 10.1016/j. foodchem.2017.07.111.
- 20 I. M. Hwang, E. W. Moon, H. W. Lee, N. Jamila, K. Su Kim, J. H. Ha and S. H. Kim, Discrimination of chili powder origin using inductively coupled plasma–mass spectrometry (ICP-MS), inductively coupled plasma–optical emission spectroscopy (ICP-OES), and near infrared (NIR) spectroscopy, *Anal. Lett.*, 2019, 52, 932–947, DOI: 10.1080/00032719.2018.1508293.
- 21 D. A. Lytle, M. R. Schock, C. Formal, C. Bennett-Stamper, S. Harmon, M. N. Nadagouda, D. Williams, M. K. Desantis, J. Tully and M. Pham, Lead particle size fractionation and identification in newark, new jersey's drinking water, *Environ. Sci. Technol.*, 2020, 54, 13672–13679, DOI: 10.1021/ acs.est.0c03797.
- 22 A. J. Borrill, N. E. Reily and J. V. Macpherson, Addressing the practicalities of anodic stripping voltammetry for heavy metal detection: A tutorial review, *Analyst*, 2019, **144**, 6834–6849, DOI: **10.1039/c9an01437c**.
- 23 Y. Lu, X. Liang, C. Niyungeko, J. Zhou, J. Xu and G. Tian, A review of the identification and detection of heavy metal ions in the environment by voltammetry, *Talanta*, 2018, 178, 324–338, DOI: 10.1016/j.talanta.2017.08.033.
- 24 C. E. Rahm, F. Torres-Canas, P. Gupta, P. Poulin and N. T. Alvarez, Inkjet printed multi-walled carbon nanotube sensor for the detection of lead in drinking water, *Electroanalysis*, 2020, 32, 1533–1545, DOI: 10.1002/ elan.202000040.
- 25 D. Zhao, D. Siebold, N. T. Alvarez, V. N. Shanov and W. R. Heineman, Carbon nanotube thread electrochemical cell: detection of heavy metals, *Anal. Chem.*, 2017, 89, 9654–9663, DOI: 10.1021/acs.analchem.6b04724.
- 26 B. Bansod, T. Kumar, R. Thakur, S. Rana and I. Singh, A review on various electrochemical techniques for heavy metal ions detection with different sensing platforms, *Biosens. Bioelectron.*, 2017, 94, 443–455, DOI: 10.1016/j. bios.2017.03.031.
- 27 A. Huseinov, B. L. Weese, B. J. Brewer and N. T. Alvarez, Near-electrode pH change for voltammetric detection of insoluble lead carbonate, *Anal. Chim. Acta*, 2021, 1186, 339087, DOI: 10.1016/j.aca.2021.339087.
- 28 P. Delahay, M. Pourbaix and P. Van Rysselberghe, Potential-pH diagram of lead and its applications to the study of lead corrosion and to the lead storage battery, *J. Electrochem. Soc.*, 1951, **98**, 57–64, DOI: **10.1149/1.2778106**.
- 29 A. F. Cantor, J. K. Park and P. Vaiyavatjamai, Effect of chlorine on corrosion in drinking water systems, *J. Am. Water*

- Works Assoc., 2003, 95, 112-122, DOI: 10.1002/j.1551-8833.2003.tb10366.x.
- 30 M. R. Schock, Response of lead solubility to dissolved carbonate in drinking water, *J. Am. Water Works Assoc.*, 1980, 72, 695–704, DOI: 10.1002/j.1551-8833.1980.tb04616.x.
- 31 P. Gupta, C. E. Rahm, D. Jiang, V. K. Gupta, W. R. Heineman, G. Justin and N. T. Alvarez, Parts per trillion detection of heavy metals in as-is tap water using carbon nanotube microelectrodes, *Anal. Chim. Acta*, 2021, 1155, 338353, DOI: 10.1016/j.aca.2021.338353.
- 32 S. Chowdhury, Water quality degradation in the sources of drinking water: an assessment based on 18 years of data from 441 water supply systems, *Environ. Monit. Assess.*, 2018, **190**(7), 379, DOI: **10.1007/s10661-018-6772-6**.
- 33 E. J. Kim, J. E. Herrera, D. Huggins, J. Braam and S. Koshowski, Effect of pH on the concentrations of lead and trace contaminants in drinking water: A combined batch, pipe loop and sentinel home study, *Water Res.*, 2011, 45, 2763–2774, DOI: 10.1016/j.watres.2011.02.023.
- 34 C. E. Boyd, C. S. Tucker and B. Somridhivej, Alkalinity and hardness: critical but elusive concepts in aquaculture, *J. World Aquacult. Soc.*, 2016, 47, 6–41, DOI: 10.1111/jwas.12241.
- 35 M. J. Brandt, M. K. Johnson, A. J. Elphinston and D. D. Ratnayaka, *Twort's water supply*, Elsevier, 7th edn, 2017. DOI: 10.1016/C2012-0-06331-4.
- 36 M. Edwards, M. R. Schock and T. E. Meyer, Alkalinity, pH, and copper corrosion by-product release, *J. Am. Water Works Assoc.*, 1996, **88**, 81–94, DOI: **10.1002/j.1551-8833.1996.tb06521.x**.
- 37 M. B. Griffith, Natural variation and current reference for specific conductivity and major ions in wadeable streams of the conterminous USA, *Freshwater Sci.*, 2014, 33, 1–17, DOI: 10.1086/674704.
- 38 R. J. Gibbs, Mechanisms controlling world water chemistry, *Science*, 1970, 170, 1088–1090, DOI: 10.1126/science.170.3962.1088.
- 39 N. Elgrishi, K. J. Rountree, B. D. McCarthy, E. S. Rountree, T. T. Eisenhart and J. L. Dempsey, A practical beginner's guide to cyclic voltammetry, *J. Chem. Educ.*, 2018, **95**, 197–206, DOI: 10.1021/acs.jchemed.7b00361.
- 40 US EPA Office of Water, Comprehensive disinfectants and disinfection byproducts rules (stage 1 and stage 2): quick reference guide, U. S. Environ. Prot. Agency, 2010, 816-F, 4. DOI: EPA 816-F-10-080.
- 41 M. P. Abdullah, L. F. Yee, S. Ata, A. Abdullah, B. Ishak and K. N. Z. Abidin, The study of interrelationship between raw water quality parameters, chlorine demand and the formation of disinfection by-products, *Phys. Chem. Earth*, 2009, 34, 806–811, DOI: 10.1016/j.pce.2009.06.014.
- 42 L. Zlatanovic, A. Moerman, J. P. van der Hoek, J. Vreeburg and M. Blokker, Development and validation of a drinking water temperature model in domestic drinking water supply systems, *Urban Water J.*, 2017, **14**, 1031–1037, DOI: **10.1080/1573062X.2017.1325501**.

- 43 S. Masters, G. J. Welter and M. Edwards, Seasonal variations in lead release to potable water, *Environ. Sci. Technol.*, 2016, **50**, 5269–5277, DOI: **10.1021/acs.** est.5b05060.
- 44 World Health Organization (WHO), Guidlines for drinkingwater quality: fourth edition incorporating the first addendum, World Health Organization, Geneva, 4th edn, 2017.
- 45 P. Gupta, R. A. Lazenby, C. E. Rahm, W. R. Heineman, E. Buschbeck, R. J. White and N. T. Alvarez, Electrochemistry of controlled diameter carbon nanotube fibers at the cross section and sidewall, ACS Appl. Energy Mater., 2019, 2, 8757–8766, DOI: 10.1021/acsaem.9b01723.
- 46 N. T. Alvarez, E. Buschbeck, S. Miller, A. D. Le, V. K. Gupta, C. Ruhunage, I. Vilinsky and Y. Ma, Carbon nanotube fibers for neural recording and stimulation, ACS Appl. Bio Mater., 2020, 3, 6478–6487, DOI: 10.1021/acsabm.0c00861.
- 47 J. Morton, N. Havens, A. Mugweru and A. K. Wanekaya, Detection of trace heavy metal ions using carbon nanotubemodified electrodes, *Electroanalysis*, 2009, 21, 1597–1603, DOI: 10.1002/elan.200904588.
- 48 G. R. Dangel, H. Kumakli, C. E. Rahm, R. White and N. T. Alvarez, Nanoelectrode ensembles consisting of carbon nanotubes, *Appl. Sci.*, 2021, 11(18), 8399, DOI: 10.3390/app11188399.
- 49 P. Gupta, C. E. Rahm, D. Jiang, V. K. Gupta, W. R. Heineman, G. Justin and N. T. Alvarez, Parts per trillion detection of heavy metals in as-is tap water using carbon nanotube microelectrodes, *Anal. Chim. Acta*, 2021, 1155, 338353, DOI: 10.1016/j.aca.2021.338353.
- 50 K. Gazica, E. FitzGerald, G. Dangel, E. N. Haynes, J. Yadav and N. T. Alvarez, Towards on-site detection of cadmium in human urine, *J. Electroanal. Chem.*, 2020, 859, 113808, DOI: 10.1016/j.jelechem.2019.113808.
- 51 X. Niu, M. Lan, H. Zhao, C. Chen, Y. Li and X. Zhu, Review: electrochemical stripping analysis of trace heavy metals using screen-printed electrodes, *Anal. Lett.*, 2013, **46**, 2479–2502, DOI: **10.1080/00032719.2013.805416**.
- 52 S. Dutta, G. Strack and P. Kurup, Gold nanostar electrodes for heavy metal detection, *Sens. Actuators, B*, 2019, **281**, 383–391, DOI: **10.1016/j.snb.2018.10.111**.
- 53 P. Podešva, I. Gablech and P. Neužil, Nanostructured gold microelectrode array for ultrasensitive detection of heavy metal contamination, *Anal. Chem.*, 2018, 90, 1161–1167, DOI: 10.1021/acs.analchem.7b03725.
- 54 G. Herzog and D. W. M. Arrigan, Determination of trace metals by underpotential deposition-stripping voltammetry at solid electrodes, *TrAC, Trends Anal. Chem.*, 2005, 24, 208–217, DOI: 10.1016/j.trac.2004.11.014.
- 55 Y. Bonfil, M. Brand and E. Kirowa-Eisner, Determination of sub-μgl-1 concentrations of copper by anodic stripping voltammetry at the gold electrode, *Anal. Chim. Acta*, 1999, 387, 85–95, DOI: 10.1016/S0003-2670(99)00066-5.
- 56 N. T. Alvarez, P. Miller, M. R. Haase, R. Lobo, R. Malik and V. Shanov, Tailoring physical properties of carbon nanotube threads during assembly, *Carbon*, 2019, 144, 55–62, DOI: 10.1016/j.carbon.2018.11.036.

- 57 N. T. Alvarez, P. Miller, M. Haase, N. Kienzle, L. Zhang, M. J. Schulz and V. Shanov, Carbon nanotube assembly at near-industrial natural-fiber spinning rates, *Carbon*, 2015, 86, 350–357, DOI: 10.1016/j.carbon.2015.01.058.
- 58 U. Kreibig and M. Vollmer, *Optical properties of metal clusters*, Springer Berlin Heidelberg, Berlin, Heidelberg, 1995. DOI: 10.1007/978-3-662-09109-8.
- 59 K. L. Kelly, E. Coronado, L. L. Zhao and G. C. Schatz, The optical properties of metal nanoparticles: The influence of size, shape, and dielectric environment, *J. Phys. Chem. B*, 2003, 107, 668–677, DOI: 10.1016/j. ocecoaman.2014.06.011.
- 60 J. A. Creighton and D. G. Eadon, Ultraviolet-visible absorption spectra of the colloidal metallic elements, *J. Chem. Soc., Faraday Trans.*, 1991, 87, 3881–3891, DOI: 10.1039/FT9918703881.
- 61 L. Wang, Z. Tang, W. Yan, H. Yang, Q. Wang and S. Chen, Porous carbon-supported gold nanoparticles for oxygen reduction reaction: effects of nanoparticle size, ACS Appl. Mater. Interfaces, 2016, 8, 20635–20641, DOI: 10.1021/ acsami.6b02223.
- 62 U. Bogdanović, I. Pašti, G. Ćirić-Marjanović, M. Mitrić, S. P. Ahrenkiel and V. Vodnik, Interfacial synthesis of gold– polyaniline nanocomposite and its electrocatalytic application, ACS Appl. Mater. Interfaces, 2015, 7, 28393–28403, DOI: 10.1021/acsami.5b09145.
- 63 Industrial Regulatory Impacts Imminent from PFAS Concerns | Trinity Consultants, (n.d.). https://www.trinityconsultants.com/news/federal/industrial-regulatoryimpacts-imminent-from-pfas-concerns (accessed November 5, 2019).
- 64 P. A. Nikolaychuk, The revised potential pH diagram for Pb H₂O system, *Ovidius Univ. Ann. Chem.*, 2018, **29**, 55–67, DOI: **10.2478/auoc-2018-0008**.
- 65 A. J. Bard and L. R. Faulkner, Electrochemical methods: fundamentals and applications, John Wiley and Sons, 2nd edn, 2001
- 66 G. March, T. Nguyen and B. Piro, Modified Electrodes Used for Electrochemical Detection of Metal Ions in Environmental Analysis, *Biosensors*, 2015, 5, 241–275, DOI: 10.3390/bios5020241.
- 67 P. T. Kissinger and W. R. Heineman, Cyclic voltammetry, *J. Chem. Educ.*, 1983, **60**, 702, DOI: **10.1021/ed060p702**.
- 68 B. Li and T. Zhang, pH significantly affects removal of trace antibiotics in chlorination of municipal wastewater, *Water Res.*, 2012, 46, 3703–3713, DOI: 10.1016/j. watres.2012.04.018.
- 69 A. Godelitsas, J. M. Astilleros, K. Hallam, S. Harissopoulos and A. Putnis, Interaction of calcium carbonates with lead in aqueous solutions, *Environ. Sci. Technol.*, 2003, 37, 3351– 3360, DOI: 10.1021/es020238i.
- 70 S. H. Smith, Temperatire correction in conductivity measurements, *Limnol. Oceanogr.*, 1962, 7, 330–334, DOI: 10.4319/lo.1962.7.3.0330.
- 71 A. A. A. Elfaki, A. A. Elamin, M. D. Abd-Alla, A. S. Mohamed, A. A. Mohamed and S. A. Elhouri, The

- Effect of Temperature on Conductivity of Conductors and Superconductors, *Am. J. Phys. Appl.*, 2017, 5(1), 1–5, DOI: 10.11648/j.ajpa.20170501.11.
- 72 D. Zhao, X. Guo, T. Wang, N. Alvarez, V. N. Shanov and W. R. Heineman, Simultaneous detection of heavy metals by anodic stripping voltammetry using carbon nanotube thread, *Electroanalysis*, 2014, 26, 488–496, DOI: 10.1002/ elan.201300511.
- 73 G. Martínez-Paredes, M. B. González-Garcaiaa and A. Costa-Garcia, Lead sensor using gold nanostructured screen-printed carbon electrodes as transducers, *Electroanalysis*, 2009, 21, 925–930, DOI: 10.1002/ elan.200804496.
- 74 B. Beverskog and I. Puigdomenech, Revised Pourbaix Diagrams for Copper at 25 to 300 °C, *J. Electrochem. Soc.*, 1997, **144**, 3476–3483, DOI: **10.1149/1.1838036**.